



# Dynamics of bubble formation in highly viscous liquid in co-flowing microfluidic device

Xiaohui Lin<sup>1</sup> · Fubing Bao<sup>1</sup> · Chengxu Tu<sup>1</sup> · Zhaoqin Yin<sup>1</sup> · Xiaoyan Gao<sup>1</sup> · Jianzhong Lin<sup>2</sup>

Received: 25 August 2018 / Accepted: 4 March 2019 / Published online: 15 April 2019  
© Springer-Verlag GmbH Germany, part of Springer Nature 2019

## Abstract

In this work, the dynamics of bubble formation in a highly viscous liquid in a co-flowing microfluidic device is experimentally investigated. The evolution of gaseous thread in the co-flowing device is recorded using a high-speed camera. The bubble formation process can be divided into three stages: retraction stage, expansion stage, and collapse stage. According to an analysis of the forces acting on the gaseous thread, the bubble formation in the co-flowing device is a competitive result of the surface tension, pressure difference and shearing effects. The surface tension effect plays an important role in the retraction stage. In the expansion stage, the pressure difference effect dominates the bubble's growth. While in the collapse stage, the shearing effect leads to the interface breakup. Three empirical correlations are proposed according to the experimental data and can be used to predict bubble formation frequency, the diameter and length of the generated bubbles.

**Keywords** Bubble formation · Highly viscous liquid · Co-flowing microfluidic device

## 1 Introduction

Microbubble formation and dynamics have attracted considerable interests during the past decade because of their wide-ranging applications in the chemical (Takahashi et al. 2007; Yue et al. 2007), material science (Yen et al. 2005), medicine (Blomley et al. 1999; Ferrara et al. 2007), ultrasonic cleaning (Kim and Kim 2014), environmental engineering (Burns et al. 1997), and mineral flotation (Calgaroto et al. 2016) industries, among others. A thorough understanding of the formation mechanism of microbubbles will provide theoretical guidance for bubble applications. Therefore,

many scholars have explored microbubble formation and its dynamic characteristics (Fu et al. 2009a; Ganan-Calvo and Gordillo 2001; Ganan-Calvo et al. 2006; Garstecki et al. 2006; Hong and Wang 2006), and research has shown that microfluidic technology is an effective bubble formation method (Koch et al. 2000; Stone et al. 2004).

The applications of microbubbles in highly viscous liquid are frequently encountered in polymer (Bloch et al. 2004; Nair et al. 2009) and food engineering (Ballestra et al. 1996; Campbell and Mougeot 1999). Liquid viscosity plays an important role in the formation of microbubbles (Lu et al. 2014; Pancholi et al. 2008a; Parhizkar et al. 2012; Wang et al. 2011). The bubble formation characteristics in highly viscous liquid have been investigated by several researchers. Burton et al. (2005) analyzed the pinch-off of nitrogen gas bubbles in a highly viscous liquid ( $\eta > 100$  cP) experimentally. The bubble neck radius was found to be proportional to the time before break, and decreases smoothly to zero. Thoroddsen et al. (2007) focused on the effects of liquid viscosity on the pinch-off speed and neck region, and the results showed that the increasing viscosity can slow down the bubble pinch-off process, lengthen the vertical spacing between the cones. Pancholi et al. (2008b) studied the formation characteristics of bubbles in a highly viscous liquid in a T-junction device and indicated that liquid viscosity has a significant

---

This article is part of the topical collection “2018 International Conference of Microfluidics, Nanofluidics and Lab-on-a-Chip, Beijing, China” guest edited by Guoqing Hu, Ting Si and Zhaomiao Liu.

---

✉ Fubing Bao  
dingobao@cjlu.edu.cn

✉ Jianzhong Lin  
mecjzlin@zju.edu.cn

<sup>1</sup> Institute of Fluid Measurement and Simulation, China Jiliang University, Hangzhou 310018, China

<sup>2</sup> Department of Mechanics, State Key Laboratory of Fluid Power Transmission and Control, Zhejiang University, Hangzhou 310027, China

influence on bubble formation and the size of the generated bubble. Bolanos-Jimenez et al. (2009) investigated the effect of liquid viscosity on the air bubble formation immersed in a stagnant liquid. Based on a Rayleigh-like pair of equations, they effectively described the bubble pinch-off process in the liquids of intermediate viscosity. Lu et al. (2016) presented the breakup dynamics of the gas–liquid interface for Taylor bubble formation in a microfluidic flow-focusing device. The results suggested that the evolution of the gas–liquid interface during bubble formation is driven by the interfacial force and possesses a self-similar shape, and the characteristic parameters for the similarity depend on the liquid viscosity. Zhang et al. (2017) reported the dynamics and mechanism of  $N_2$  bubble formation in highly viscous glycerol–water mixtures in a flow-focusing device. The evolution of the volume of the gaseous thread during bubble formation was also recorded and analyzed.

Among different microfluidic bubble generation devices, co-flowing technology has the advantage of easy processing, easy assembly, and reusability and has been adopted by many researchers to generate bubbles for different purposes. Castro-Hernández et al. (2011) reported that the microbubbles produced in a co-flow device is a function of viscosity ratio and liquid flow rate ratio, and they also claimed that the pressure gradient in the entrance region is the reason for bubble formation in low viscosity liquids. Van Hoeve et al. (2011) proposed the equation to predict the radius of gas jets in co-flowing streams and stated that flow rate ratio and outer tube radius are the control parameters. For bubble formation in coflowing devices using low viscosity liquids (like water), liquid inertia dominates over viscous and surface tension forces at large Reynolds and Weber number (Rodríguez-Rodríguez et al. 2015). However, Zhang et al. (2014) found that the sizes of bubbles generated in a novel co-flow-focusing device are controlled by the liquid flow rate and liquid viscosity, and the existence of a shear stress is one key ingredient for bubble formation. Moreover, Li et al. (2017) studied microbubble formation using a capillary tube surrounded by a co-flowing liquid in a mechanically assembled microfluidic chip and developed a modified two-stage model for the prediction of microbubble formation. Wang et al. (2013) investigated the mechanism of bubble formation in coaxial streams using different dispersed-phase gases and different concentrations of continuous-phase liquids and analyzed their influences on bubble size. Bhunia et al. (1998) analyzed the roles of multiple forces in the process of bubble formation in coaxial flow, and an overall force balance describing bubble dynamics was developed. Wang (2015) numerically studied the microbubble formation characteristics in coaxial flow and focused on the dynamic process of bubble formation under Taylor flow.

The influence of gas nozzle length on the formation of bubbles was also demonstrated.

Although many efforts have been devoted to the bubble formation mechanism and the prediction of bubble size in co-flowing devices, most of these studies have focused on bubble formation in low viscous fluids, and the breakup mechanism in the bubble formation has been debated (Anna 2016). Studies on the bubble formation in highly viscous liquids have been carried out in micro flow-focusing and T-junction devices. Therefore, it is necessary to investigate the mechanism and dynamics of bubble formation in highly liquid in co-flowing device. In the present work, a comprehensive study of the dynamics of bubble formation in highly viscous liquid in a co-flowing microfluidic device is carried out. The remainder of this paper is organized as follows. Section 2 demonstrates the experimental setups. Section 3 describes the detailed bubble generation process and dynamics. Finally, Sect. 4 elaborates the conclusions of the study.

## 2 Experimental setup

The experimental system for bubble generation is shown in Fig. 1. This installation is mainly composed of a nitrogen cylinder, a syringe pump (Harvard Pump 11 Elite), a co-flowing microfluidic chip, an inverted microscope (Nikon Eclipse Ti-S), and a high-speed camera (NAC MEMRE-CAM HX-6). The high-speed camera runs at a frame rate of up to 10 kHz in all present experiments, which can take approximately 400–900 images within a single bubble formation cycle. The inlet gas pressure is controlled and stabilized by a pressure regulator (SMC IR2010) and a gas tank.

The co-flowing microfluidic chip is fabricated by inserting two nested glass capillaries, an injection capillary and a collection capillary, in a square-section glass channel, as shown in Fig. 2. The gap between the collection capillary and square-section glass channel is blocked to ensure that the liquid and generated bubbles flow through the collection capillary. Hence, the co-flowing microfluidic chip includes

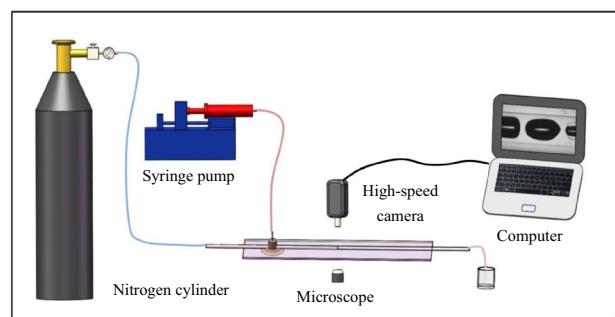
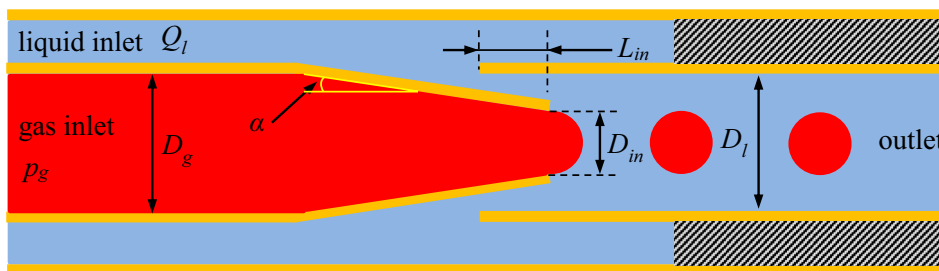


Fig. 1 Schematic of the experimental setup

**Fig. 2** Schematic of the co-flowing microfluidic chip



an inner coaxial gas inlet, an outer coaxial liquid inlet, and a two-phase outlet. The internal diameters of the injection and collection capillaries,  $D_g$  and  $D_l$ , respectively, are both  $550\ \mu\text{m}$ . The internal diameter of the injection nozzle  $D_{in}$  is  $165\ \mu\text{m}$ , and the length of the insert  $L_{in}$  is  $340\ \mu\text{m}$ . The inclination angle of the tapered nozzle  $\alpha$  is  $5^\circ$ .

Glycerol ( $\eta = 1172\ \text{mPa}\cdot\text{s}$ ,  $\rho = 1.26\ \text{g}/\text{cm}^3$ ) is chosen as the continuous phase and nitrogen (99.99%) is used as the disperse phase. The viscosity of glycerol is much larger than that of low viscous fluid; that is, the viscosity of water is  $1.01\ \text{mPa}\cdot\text{s}$  at  $20\ ^\circ\text{C}$ . The surface tension  $\gamma$  is  $63.70\ \text{mN}/\text{m}$ . The viscosity and surface tension are measured using a viscometer (Lichen NDJ-5S) and a Wilhelmy plate tensiometer (Shanghai BYZ-2), respectively. All the experiments are carried out at a room temperature of  $20 \pm 0.5\ ^\circ\text{C}$ .

The generated bubbles in the channel are not spherical because of the viscous shear force and pressure difference

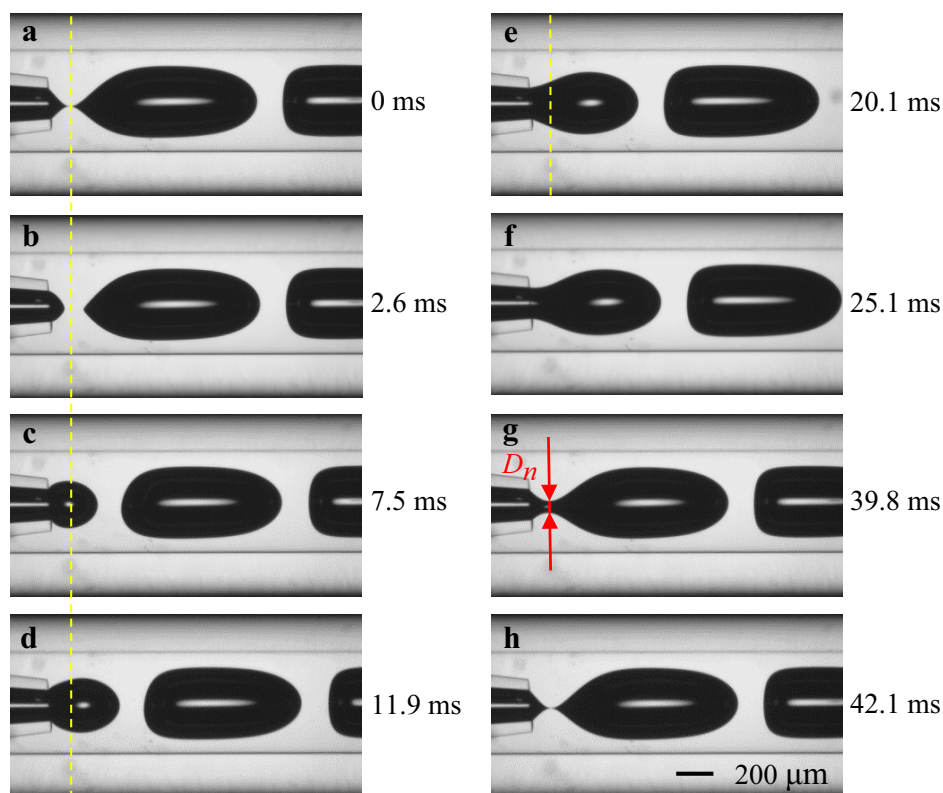
between the inlet and outlet. To measure the bubble diameter, the non-spherical bubbles are collected within a glass culture dish, because the nitrogen bubbles are relatively stable in glycerol. Thus, spherical bubbles can be achieved and the bubble diameter can then be measured, by taking into consideration the pressure difference. Five measurements are repeated and the average value is adopted to guarantee measurement accuracy.

### 3 Results and discussion

#### 3.1 Bubble formation process

A typical bubble formation cycle in the co-flowing microfluidic device is shown in Fig. 3. The shape evolution of the gaseous thread is recorded using the high-speed camera. The

**Fig. 3** Typical bubble formation cycle when  $p_g = 100\ \text{kPa}$ ,  $Q_l = 3.7\ \text{mL}/\text{h}$



pressure of the gas inlet is set to 100 kPa, and the flow rate of the liquid inlet is 3.7 mL/h. The bubble formation period is approximately 42.1 ms.

In the present study, the breakup moment of the gaseous thread with the inlet gas in the bubble formation process is chosen as the starting point of the new bubble formation cycle, as shown in Fig. 3a. This instantaneous time is recognized as 0 ms. The gaseous thread retracts upstream after the breakup because of the surface tension effect. Then, the thread begins to expand quickly as a result of the high gas pressure in the injection capillary. With the expansion of the gaseous thread, a neck begins to appear, as shown in Fig. 3g, and the diameter of the neck gradually decreases. Finally, the gaseous thread neck collapses sharply and a single bubble is generated.

To quantify the bubble formation characteristics, the gaseous thread neck is defined, located at the minimum diameter between the injection capillary and gaseous thread, as can be seen in Fig. 3g. However, at the beginning of the bubble expansion process, the gaseous thread is ellipsoid and no neck can be found, as shown in Fig. 3c–e. So, a reference position, the breakup position, is defined as the neck, as shown in Fig. 3, the yellow dashed line. The diameter of gaseous thread at the neck is recognized as  $D_n$ . The variation of bubble neck diameter with time is shown in Fig. 4.

As shown in Figs. 3 and 4, the bubble generation period can be divided into three stages. In Stage I, the thread retracts upstream, as a result of the surface tension force, and the edge of gaseous thread moves to the left until it reaches the closest position to the gas inlet (Fig. 3b). According to the definition of bubble neck position, the diameter of bubble neck is 0, as shown in Fig. 3a, b. The surface tension

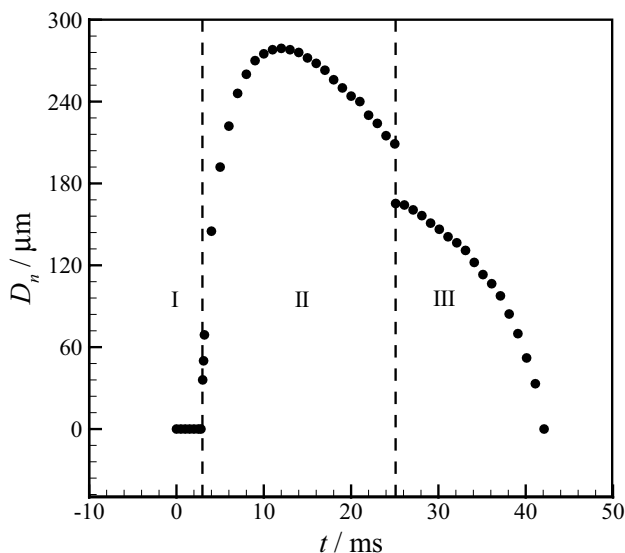


**Fig. 4** Temporal evolution of the gaseous thread neck diameter within a typical bubble formation cycle when  $p_g = 100$  kPa,  $Q_l = 3.7$  mL/h

force dominates the bubble generation behavior in this stage. Then, the thread edge starts to move downstream and the bubble formation process enters Stage II. In this stage, the pressure inside the gaseous thread is larger than that of the surrounding liquid. As a result, the gaseous thread expands quickly. At the beginning of Stage II, the gaseous thread does not reach the reference position; hence, the neck diameter is still 0. Gradually, the thread exceeds the reference position and, thus, the thread neck diameter begins to increase rapidly and reaches its maximum. Because of the geometry limitation, the gaseous thread expands toward downstream and the neck diameter decreases gradually later. When the neck of gaseous thread appears, the bubble formation process enters Stage III. With the further expansion of the gaseous thread, the gap between the gaseous thread and the collection capillary wall becomes smaller. As a result, the velocity gradient near the gaseous thread interface is larger and so is the shear stress. Meanwhile, the gaseous thread surface becomes larger with the expansion of the gaseous thread. The viscous shear force on the bubble towards downstream increases. The gaseous thread begins to collapse and the diameter of the neck decreases. When the gaseous thread breaks, a single bubble is generated and a new bubble formation cycle begins. The bubble formation process in the co-flowing microfluidic device is similar to that in flow-focusing devices (Anna 2016; Dietrich et al. 2008). However, the maximum diameter of the gaseous thread neck is larger than the gas inlet diameter, which is different from the results of Lu et al. (2014) and Zhang et al. (2017) in microfluidic flow-focusing devices.

### 3.2 Force analysis of gaseous thread

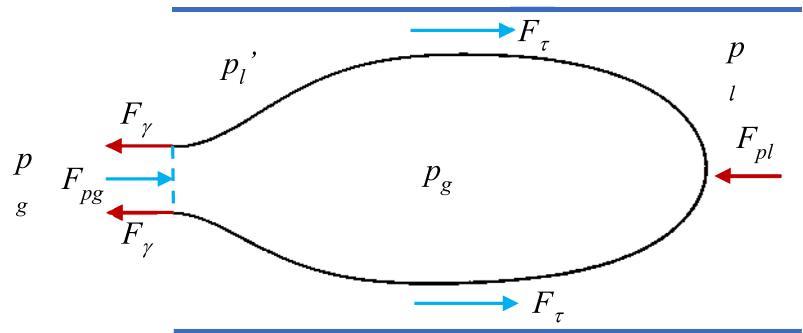
To reveal the underlying mechanism of the bubble formation difference between highly viscous and low viscous liquids, the forces acting on the gaseous thread during the bubble formation are analyzed, as shown in Fig. 5. The gaseous thread is truncated at the neck. The resultant force on the gaseous thread can be expressed as follows:

$$F = F_\tau + F_\gamma + F_{pg} + F_{pl} + F_g + F_b, \quad (1)$$

where  $F_\tau$  is the viscous shear force,  $F_\gamma$  is the surface tension force,  $F_{pg}$  is the pressure force on the inner surface of the thread from the gas, and  $F_{pl}$  is the pressure force on the outer surface from the liquid.  $F_g$  represents the gravity force and  $F_b$  represents the buoyancy force. These two forces are relatively small and thus are neglected in our present analysis.

For the bubble formation in highly viscous liquid, the gaseous thread does not obstruct the entire cross section of the microchannel so that the viscous liquid can pass through the gap between the gaseous thread and collection capillary wall. A velocity gradient exists near the gaseous thread

**Fig. 5** Forces acting on the gaseous thread during the bubble formation



surface. Thus, the viscous shear force acting on the gaseous thread can be expressed as:

$$F_\tau = \int \mu \frac{\partial u}{\partial n} ds, \tag{2}$$

where  $n$  represents the normal direction of the thread surface and  $ds$  is the unit surface area. Because of the axial symmetry, only viscous shear force in the flow direction exists. The viscous shear force is conducive to the bubble formation. The velocity gradient increases with the increase in inlet liquid flow rate. As a result, the viscous shear force increases with the inlet liquid flow rate. Equation (2) also shows that the viscous shear force is directly proportional to the gaseous thread surface. Therefore, the shear force increases continuously with the growth of the gaseous thread during the whole process of bubble generation.

The surface tension force in Eq. (1) can be expressed as:

$$F_\gamma = 2\pi D_e \gamma, \tag{3}$$

where  $D_e$  is the effective diameter, in Stage I and Stage II, the  $D_e$  is equal to the internal diameter of the injection nozzle  $D_{in}$ , while in Stage III the  $D_e$  is equal to thread neck diameter  $D_n$ . As shown in Fig. 6, the surface tension is along the opposite flow direction. Its effect pulls the gaseous thread back to the injection capillary. Therefore, this force is not conducive to the bubble formation. Due to the surface tension, the gaseous thread retracts to the upstream after the breakup. In our present study,  $\gamma$  is a constant. Therefore, the surface tension force keeps constant during Stages I and II of bubble formation, and decreases with the decrease of gaseous thread neck diameter in Stage III.

The gas pressure inside the gaseous thread is recognized as  $p_g$ . This pressure is different from the inlet gas pressure, with a difference of  $\Delta p_g$ , which is the pressure loss when the inflow gas flows from the inlet to the nozzle. This pressure loss is a function of injection capillary geometry and gas property.  $p_g$  may vary in the gaseous thread, but this variation is small and can be neglected. As shown in Fig. 6, the liquid pressure near the front part of the gaseous thread is  $p_l$ , and the liquid pressure near the thread neck is defined

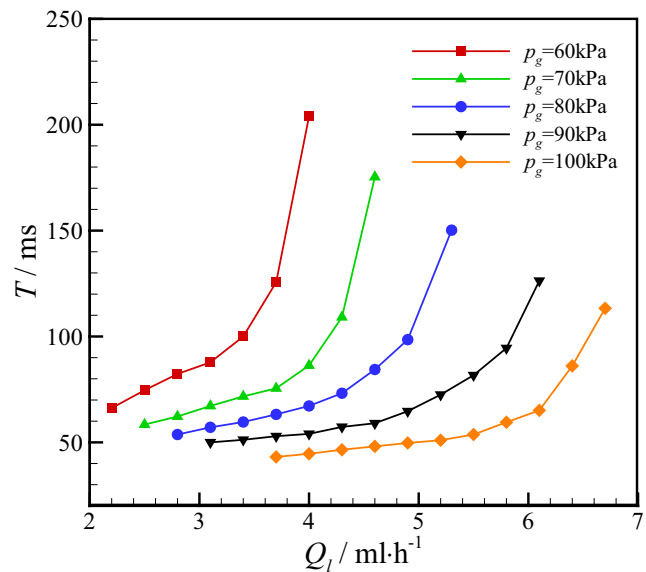


**Fig. 6** Variations of bubble formation period with inlet gas pressure and liquid flow rate

as  $p_l'$ .  $p_l$  and  $p_l'$  may be in great difference. In some bubble formation in low viscous liquids, the bubble may obstruct the whole tube. Therefore,  $p_l'$  may be much larger than  $p_l$ . A large pressure difference effect occurs in this situation. However, in our present study, the gap between the gaseous thread and collection capillary wall is large. The pressure difference between  $p_l$  and  $p_l'$  can also be neglected. Because of the axial symmetry of the gaseous thread, the resultant pressure force on the inner surface from the gas exists only in the flow direction and can be written as:

$$F_{pg} = \frac{\pi}{4} D_e^2 p_g. \tag{4}$$

Similarly, the pressure force on the outer surface from the liquid can be written as:

$$F_{pl} = \frac{\pi}{4} D_e^2 p_l, \tag{5}$$



where  $p_1$  is the liquid pressure near the gaseous thread. In our present study, the gas and liquid pressure inside and outside the gaseous thread is considered to be homogeneous. In our experiments, the collection capillary is connected to a polythene tube with an internal diameter of 1 mm. The polythene tube is then discharged directly to the atmosphere. Thus,  $p_1$  is the pressure loss of liquid flow from the nozzle to the polythene tube outlet:

$$p_1 = \Delta p_{11} + \Delta p_{12} = \frac{128\mu L_1}{\pi D_1^4} Q_1 + \frac{128\mu L_2}{\pi D_2^4} Q_1, \quad (6)$$

where  $\Delta p_{11}$  and  $\Delta p_{12}$  represent the pressure losses in the collection capillary and polythene tube, respectively;  $L_1$  and  $L_2$  are the lengths of the collection capillary and polythene tube, respectively; and  $D_2$  is the internal diameter of the polythene tube. In our experiment,  $L_1$  and  $L_2$  are 5.5 and 7.4 cm, respectively. When these parameters are substituted, Eq. (6) becomes:

$$p_1 = \Delta p_{11} + \Delta p_{12} = (3.23 \times 10^{13}) Q_1 \frac{\text{Pa s}}{\text{m}^3}.$$

When  $Q_1$  is 6.7 mL/h, the pressure outside the gaseous thread is approximately 64.9 kPa. This background pressure is already higher than the inlet pressure of 60 kPa. In this situation, no bubble can be generated and the bubble formation period is infinite.

In a low viscous liquid flow, the liquid viscosity is at the order of 1 mPa s (Dietrich et al. 2008), so  $p_1$  is much smaller than  $p_g$  and  $F_{pl}$  can thus be neglected. However, in the present highly viscous liquid flow, the liquid viscosity is 1172 mPa s, which is three orders of magnitude larger than the low viscous liquid. The pressure loss in the collection capillary and polythene tube is at the same order of magnitude as the inlet gas pressure.

According to Eqs. (4) and (5), the combined effect of pressure force ( $F_{pg} - F_{pl}$ ) also keeps constant during Stage I and Stage II, and then decreases rapidly with the decrease of thread neck diameter in Stage III.

The bubble formation process is a competitive result of the surface tension (surface tension force,  $F_\gamma$ ), pressure difference (normal pressure force on the gaseous thread surface,  $F_{pg} - F_{pl}$ ) and shearing (viscous shear force,  $F_\tau$ ) effects. The surface tension is a constant when the continuous and disperse phases are chosen. The surface tension force plays an important role in the retraction stage. In the expansion stage, the pressure difference effect dominates the bubble's growth. While in the collapse stage, with the increases of viscous shear force and the gaseous thread surface, the shearing effect leads to the interface breakup.

### 3.3 Bubble formation period

The bubble formation period  $T$  in the co-flowing microfluidic device is then investigated. The variations of the bubble formation period with liquid flow rate at different inlet gas pressures are shown in Fig. 6. Five inlet gas pressures (60, 70, 80, 90 and 100 kPa) are studied. As shown in the figure, the bubble formation period increases with the increase of inlet liquid flow rate for a given inlet gas pressure. The bubble formation period increases linearly with the increase of liquid flow rate first. However, it increases rapidly when the liquid flow rate reaches a certain critical value for all five inlet pressures. These critical values vary at different inlet gas pressures. This is consistent with the theoretical analysis in Eq. (6). When  $Q_1$  is 6.7 mL/h, the pressure outside the gaseous thread is approximately 64.9 kPa, which is already higher than the inlet pressure of 60 kPa. No bubble can be generated and the bubble formation period is infinite. This analysis is validated by the experimental data, which are shown in Fig. 6. This phenomenon is interesting and is different from the results obtained at low/intermediate liquid viscosity (Fu et al. 2009b; Li et al. 2017; Zhang et al. 2014). In their experiments, the bubble formation period decreases gradually when the liquid flow rate increases.

The bubble formation frequencies at different inlet gas pressures and flow rates are shown in Fig. 7. According to the experimental data, the following relationship between the bubble formation frequency and operating conditions can be achieved:

$$f = 0.38 \ln(Re_g Re_l) + 2.57, \quad (7)$$

where  $f$  is the dimensionless bubble formation frequency, non-dimensionalized with  $4Q_1/\pi D_1^3$ .  $Re_g$  and  $Re_l$  are Reynolds number defined according to the gas inlet and liquid inlet, respectively:

$$Re_g = \frac{\rho_g Q_g}{\pi \mu_g D_{in}}, \quad (8)$$

$$Re_l = \frac{\rho_l Q_l}{\pi \mu_l D_1}, \quad (9)$$

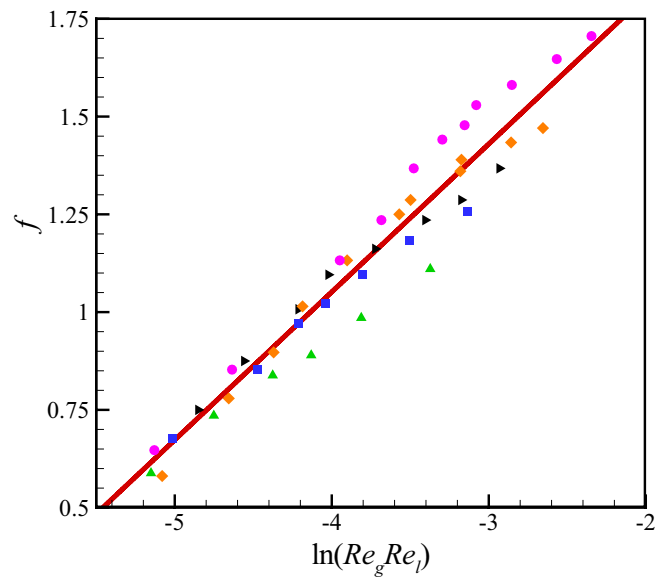
where  $Q_1$  is the inlet liquid flow rate and  $Q_g$  is the inlet gas flow rate:

$$Q_g = f V_b, \quad (10)$$

where  $V_b$  is the volume of a single bubble.

Bubble generation frequency linearly increases with the increase in the product of Reynold numbers for gas inlet and liquid inlet. Equation (7) can be used to predict the bubble formation frequencies at different inlet conditions.

**Fig. 7** Variation of bubble formation frequency with inlet gas pressure and flow rate



**3.4 Generated bubble size**

In microfluidic flows, Weber number ( $We$ ):

$$We = \frac{\rho D u^2}{\gamma}, \tag{11}$$

and capillary number ( $Ca$ ):

$$Ca = \frac{\mu u}{\gamma}, \tag{12}$$

are usually used to analyze the flow dynamics. In our experiments, according to the geometry and flow conditions, the range of  $Re$  is approximately  $10^{-3}$  to  $10^0$ , and the range of  $We$  is approximately  $10^{-8}$  to  $10^{-4}$ , indicating that the inertial force is small compared with the viscous and surface tension forces. The range of  $Ca$  is approximately 0.1–0.4, which means that the viscous and surface tension forces should both be considered.

The generated bubble sizes at different operating conditions are then investigated. The bubble diameter is nondimensionalized with the internal diameter of the injection nozzle, that is,  $D_{in}$ . The effects of gas–liquid flow rate ratio  $\varphi = Q_g/Q_l$  and the  $Ca$  number are explored. The empirical correlation proposed by Cubaud and Mason (2008), which is used to predict the dripping droplet size in a square microchannel, is used for reference in the present study. The nondimensional bubble diameter is considered a function of the product of gas–liquid flow rate ratio and capillary number  $Ca$ . From the experimental data, the following correlation for the bubble diameter can be obtained:

$$\frac{D_b}{D_{in}} = 4(\varphi Ca)^{0.16}. \tag{13}$$

This correlation is similar to that in bubble generation in low viscous liquid in microfluidics devices (Cubaud and Mason 2008; Lu et al. 2014). However, the coefficient and exponent in Eq. (13) are different. Furthermore, the exponents for the gas–liquid flow rate ratio and capillary number are different in their correlations, but in our study, the gas–liquid flow rate ratio and capillary number are united and have the same exponent. The variation of the generated bubble diameter with  $Ca$  is shown in Fig. 8. As shown in the figure, the nondimensional bubble diameter increases with the increase of the product of gas–liquid flow rate ratio and capillary number. Thus, the empirical correlation agrees well with the experimental data.

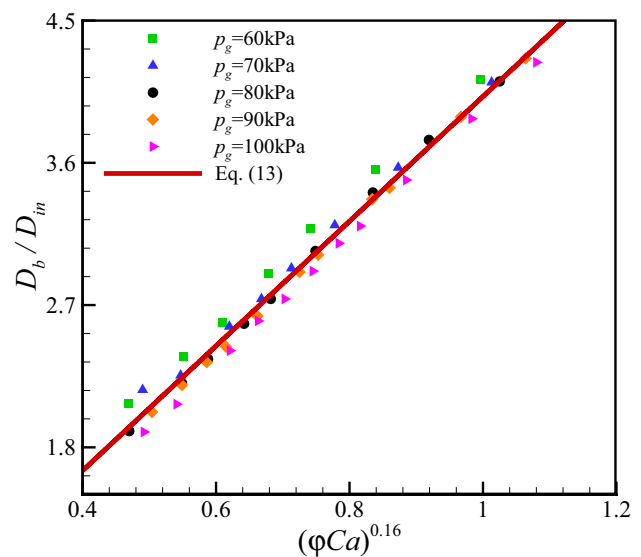


**Fig. 8** Variation of nondimensional bubble diameter with  $\varphi Ca$

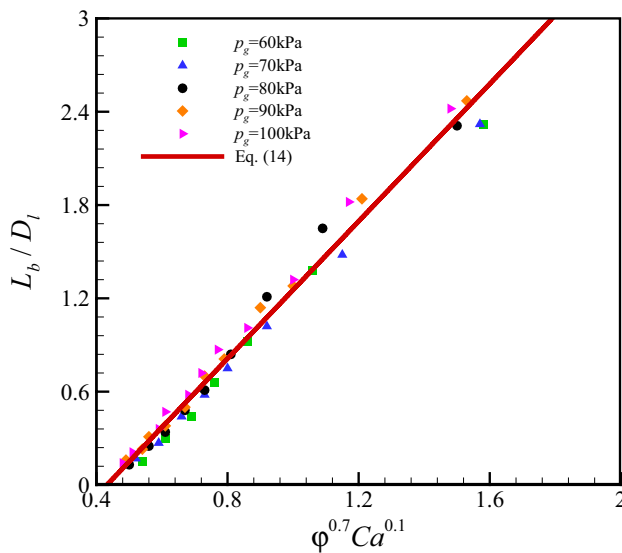


**Fig. 9** Variation of the nondimensional bubble length with gas–liquid flow rate ratio

The generated bubbles are not spherical, as shown in Fig. 3. The bubbles mostly have bullet-shaped tops because of the viscous shear force and the pressure difference in the channel, as shown in Fig. 3e. The curvature radius at the front part of the bubble is usually smaller than that at the rear part. The length of the bubble  $L_b$  in the flow direction is a function of the operating conditions. The variation of the nondimensional bubble length, which is nondimensionalized using the diameter of the collection capillary, with gas–liquid flow rate ratio is shown in Fig. 9. As shown in the figure, the bubble length increases with the increase in the gas–liquid flow rate ratio. A power law fitting correlation, obtained from the experimental data:

$$\frac{L_b}{D_1} = 2.2\phi^{0.7}Ca^{0.1}, \quad (14)$$

is also shown in the figure. Equation (14) is similar to the empirical relationships obtained from the bubble generation in micro-flow-focusing and T-junction devices (Fu et al. 2010; Tan et al. 2008; Xu et al. 2008; Zhang et al. 2017). However, the exponent in Eq. (14) is different. The difference can be attributed to the geometry of the channel, operating conditions, and liquid viscosity. The present fitting correlation agrees well with the experimental data and can be used to predict the bubble generation in the co-flowing microfluidic devices. The effect of capillary number on the bubble length can be ignored, as in the work of Zhang et al. (2017).

## 4 Conclusions

The bubble formation dynamics in highly viscous liquid in a co-flowing microfluidic device are investigated in detail in this research. The shape evolution of the gaseous thread is recorded and discussed. The bubble formation period increases with the increase in the inlet liquid flow rate, which is different from the results at a low liquid viscosity. The bubble formation process can be divided into three stages: retraction stage, expansion stage, and collapse stage. The bubble formation process is a competitive result of the surface tension (surface tension force), pressure difference (normal pressure force on the gaseous thread surface) and shearing (tangential viscous shear force on the gaseous thread surface) effects. The surface tension effect plays an important role in the retraction stage. In the expansion stage, the pressure difference effect dominates the bubble's growth. While in the collapse stage, with the increase in viscous shear force and the gaseous thread surface, the shearing effect leads to the interface breakup. Finally, the corrections of the bubble generation frequency, diameter and length of the generated bubble with gas–liquid flow rate ratio, capillary number, and flow rate are proposed. The present study will help in the understanding of the formation mechanism of microbubbles and provide theoretical guidance for bubble applications.

**Acknowledgements** This work was supported by the National Natural Science Foundation of China (Grant nos. 11672284 and 11602266) and the National Key R&D Program of China (Grant no. 2017YFB0603701).

## References

- Anna SL (2016) Droplets and bubbles in microfluidic devices. *Annu Rev Fluid Mech* 48:285–309
- Ballestra P, Da Silva AA, Cuq J (1996) Inactivation of *Escherichia coli* by carbon dioxide under pressure. *J Food Sci* 61:829–831
- Bhunia A, Pais SC, Kamotani Y, Kim IH (1998) Bubble formation in a coflow configuration in normal and reduced gravity. *AIChE J* 44:1499–1509
- Bloch SH, Wan M, Dayton PA, Ferrara KW (2004) Optical observation of lipid-and polymer-shelled ultrasound microbubble contrast agents. *Appl Phys Lett* 84:631–633
- Blomley MJ et al (1999) Improved imaging of liver metastases with stimulated acoustic emission in the late phase of enhancement with the US contrast agent SH U 508A: early experience. *Radiology* 210:409–416
- Bolanos-Jiménez R, Sevilla A, Martínez-Bazán C, Van Der Meer D, Gordillo JM (2009) The effect of liquid viscosity on bubble pinch-off. *Physics of fluids* 21:072103
- Burns S, Yiacoumi S, Tsouris C (1997) Microbubble generation for environmental and industrial separations. *Sep Purif Technol* 11:221–232
- Burton JC, Waldrep R, Taborek P (2005) Scaling and instabilities in bubble pinch-off. *Phys Rev Lett* 94:184502



- Calgaroto S, Azevedo A, Rubio J (2016) Separation of amine-insoluble species by flotation with nano and microbubbles. *Miner Eng* 89:24–29
- Campbell GM, Mougeot E (1999) Creation and characterisation of aerated food products. *Trends Food Sci Technol* 10:283–296
- Castro-Hernández E, W VH DL, Gordillo JM (2011) Microbubble generation in a co-flow device operated in a new regime. *Lab Chip* 11:2023–2029
- Cubaud T, Mason TG (2008) Capillary threads and viscous droplets in square microchannels. *Phys Fluids* 20:053302
- Dietrich N, Poncin S, Midoux N, Li HZ (2008) Bubble formation dynamics in various flow-focusing microdevices. *Langmuir* 24(24):13904–13911
- Ferrara K, Pollard R, Borden M (2007) Ultrasound microbubble contrast agents: fundamentals and application to gene and drug delivery. *Ann Rev Biomed Eng* 9:415–447
- Fu T, Funfschilling D, Ma Y, Li HZ (2009a) Scaling the formation of slug bubbles in microfluidic flow-focusing devices. *Microfluid Nanofluid* 8:467–475
- Fu T, Ma Y, Funfschilling D, Li HZ (2009b) Bubble formation and breakup mechanism in a microfluidic flow-focusing device. *Chem Eng Sci* 64:2392–2400
- Fu T, Ma Y, Funfschilling D, Zhu C, Li HZ (2010) Squeezing-to-dripping transition for bubble formation in a microfluidic T-junction. *Chem Eng Sci* 65:3739–3748
- Ganan-Calvo AM, Gordillo JM (2001) Perfectly monodisperse microbubbling by capillary flow focusing. *Phys Rev Lett* 87:274501
- Ganan-Calvo AM, Herrada MA, Garstecki P (2006) Bubbling in unbounded coflowing liquids. *Phys Rev Lett* 96:124504
- Garstecki P, Fuerstman MJ, Stone HA, Whitesides GM (2006) Formation of droplets and bubbles in a microfluidic T-junction—scaling and mechanism of break-up. *Lab Chip* 6:437–446
- Hong Y, Wang F (2006) Flow rate effect on droplet control in a coflowing microfluidic device. *Microfluid Nanofluid* 3:341–346
- Kim T-H, Kim H-Y (2014) Disruptive bubble behaviour leading to microstructure damage in an ultrasonic field. *J Fluid Mech* 750:355–371
- Koch M, Evans A, Brunnschweiler A, Evans A, Brunnschweiler A (2000) *Microfluidic technology and applications*. Research Studies Press, Philadelphia
- Li P, Zhang H, Jiang S, Qin H, Ren Y, Sun L (2017) Microbubble formation in a co-flowing liquid in a microfluidic chip. *Chem Eng Technol* 40:1512–1521
- Lu Y, Fu T, Zhu C, Ma Y, Li HZ (2014) Scaling of the bubble formation in a flow-focusing device: role of the liquid viscosity. *Chem Eng Sci* 105:213–219
- Lu Y, Fu T, Zhu C, Ma Y, Li HZ (2016) Experimental investigation on the breakup dynamics for bubble formation in viscous liquids in a flow-focusing device. *Chem Eng Sci* 152:516–527
- Nair A, Thevenot P, Dey J, Shen J, Sun M-W, Yang J, Tang L (2009) Novel polymeric scaffolds using protein microbubbles as porogen and growth factor carriers. *Tissue Eng Part C* 16:23–32
- Pancholi K, Stride E, Edirisinghe M (2008a) Dynamics of bubble formation in highly viscous liquids. *Langmuir* 24:4388–4393
- Pancholi KP, Farook U, Moaleji R, Stride E, Edirisinghe MJ (2008b) Novel methods for preparing phospholipid coated microbubbles. *Eur Biophys J* 37:515–520
- Parhizkar M, Edirisinghe M, Stride E (2012) Effect of operating conditions and liquid physical properties on the size of monodisperse microbubbles produced in a capillary embedded T-junction device. *Microfluid Nanofluid* 14:797–808
- Rodríguez-Rodríguez J, Sevilla A, Martínez-Bazán C, Gordillo JM (2015) Generation of microbubbles with applications to industry and medicine. *Annu Rev Fluid Mech* 47:405–429
- Stone HA, Stroock AD, Ajdari A (2004) Engineering flows in small devices: microfluidics toward a lab-on-a-chip. *Annu Rev Fluid Mech* 36:381–411
- Takahashi M, Chiba K, Li P (2007) Free-radical generation from collapsing microbubbles in the absence of a dynamic stimulus. *J Phys Chem B* 111:1343–1347
- Tan J, Xu J, Li S, Luo G (2008) Drop dispenser in a cross-junction microfluidic device: scaling and mechanism of break-up. *Chem Eng J* 136:306–311
- Thoroddsen ST, Etoh TG, Takehara K (2007) Experiments on bubble pinch-off. *Phys Fluids* 19:042101
- van Hoeve W, Dollet B, Gordillo JM, Versluis M, Lv W, Lohse D (2011) Bubble size prediction in co-flowing streams. *Europhys Lett* 94:64001
- Wang ZL (2015) Speed up bubbling in a tapered co-flow geometry. *Chem Eng J* 263:346–355
- Wang K, Lu YC, Xu JH, Tan J, Luo GS (2011) Generation of micromonodispersed droplets and bubbles in the capillary embedded T-junction microfluidic devices. *AIChE J* 57:299–306
- Wang K, Xie L, Lu Y, Luo G (2013) Generating microbubbles in a coflowing microfluidic device. *Chem Eng Sci* 100:486–495
- Xu J, Li S, Tan J, Luo G (2008) Correlations of droplet formation in T-junction microfluidic devices: from squeezing to dripping. *Microfluid Nanofluid* 5:711–717
- Yen BKH, Günther A, Schmidt MA, Jensen KF, Bawendi MG (2005) A microfabricated gas-liquid segmented flow reactor for high-temperature synthesis: the case of CdSe quantum dots. *Angew Chem* 117:5583–5587
- Yue J, Chen G, Yuan Q, Luo L, Gonthier Y (2007) Hydrodynamics and mass transfer characteristics in gas-liquid flow through a rectangular microchannel. *Chem Eng Sci* 62:2096–2108
- Zhang JM, Li EQ, Thoroddsen ST (2014) A co-flow-focusing monodisperse microbubble generator. *J Micromech Microeng* 24:035008
- Zhang C, Fu T, Zhu C, Jiang S, Ma Y, Li HZ (2017) Dynamics of bubble formation in highly viscous liquids in a flow-focusing device. *Chem Eng Sci* 172:278–285

**Publisher's Note** Springer Nature remains neutral with regard to jurisdictional claims in published maps and institutional affiliations.